Letter Vol. 49, No. 4 / 15 February 2024 / Optics Letters 1029

Optics Letters

Directional emission of a three-dimensional connection-type metamaterial

JIA-YI LIU, JIAN-WEN DONG, AND WEN-JIE CHEN*

School of Physics & State Key Laboratory of Optoelectronic Materials and Technologies, Sun Yat-sen University, Guangzhou 510275, China
**chenwj5@mail.sysu.edu.cn*

Received 9 January 2024; accepted 27 January 2024; posted 1 February 2024; published 12 February 2024

Directional emission of electromagnetic waves plays an essential role in laser radar and free-space communication. For most directional antennas, bandwidth and miniaturization are a pair of contradictions due to their underlying interference mechanism. Connection-type metamaterials exhibit exotic electromagnetic response near zero-frequency, which relies on the global topology of mesh connectivity rather than resonance and thus has a broad working bandwidth. In this Letter, we investigate the broadband orientation-dependent coupling effect of a 3D double mesh metamaterial. Based on this effect, we achieve a broadband directional emission (relative bandwidth of 37.72%) using a compact structure (compared to twice working wavelength). Our work provides a novel, to the best of our knowledge, scheme to manipulate a long-wavelength wave and may pave the way to a miniaturized directional antenna.

https://doi.org/10.1364/OL.518314

Directional emission of an electromagnetic (EM) wave, which refers that the EM energy is emitted in a specific and focused direction, has a widespread application in laser radar and free-space communication. A common approach to achieve a directional emission is based on the directional antenna. Dipole antennas, Yagi antennas, log-periodic antennas, etc. are widely applied in the microwave range (0.1 mm–1 m) for EM communication between mobile terminals and relay stations. However, their bandwidth and miniaturization are a pair of contradictions and are mutually exclusive. Most compact antennas (including microstrip antennas and dipole antennas) work around the resonant frequency with finite bandwidth, whereas, broadband antennas (e.g., log-periodic antennas) are too bulky for miniaturization because they are composed of a series of dipole elements working at different frequencies.

Metamaterials are one type of artificially synthesized microstructures made from assemblies of subwavelength resonant elements [1–6]. Due to their unique equifrequency surfaces, they can exhibit plenty of exotic and unnatural EM phenomena, such as negative refraction [3,7,8], perfect lens [9–11], and EM cloaking [12–14]. In the past decade, researchers have proposed and demonstrated directional emission based on zero-index metamaterials [15,16] and hyperbolic metamaterials [17]. But since the unnatural EM response of these metamaterials relies on EM resonance of resonant elements, these directional emission mechanisms only work around finite frequency [1,2]. When an EM wave frequency approaches zero (long-wavelength limit), such types of resonant metamaterials degrade into natural media with a positive refractive index. Correspondingly, their equifrequency surface is reduced into usual ellipsoids centered at zero **k**-point. Recently, researchers found that connection-type metamaterials, constructed from multiple sets of interpenetrating meshes [18–32], can exhibit an unnatural EM response near zero-frequency and thus have broader relative bandwidth. The reason is that their exotic EM response stems from the global connectivity of the interlaced meshes rather than from the EM resonance of individual metallic elements. Their equifrequency surface comes in an index ellipsoid centered at nonzero **k**-points even for a long-wavelength limit [26].

In this study, we investigate the orientation-dependent coupling effect of a 3D connection-type metamaterial. On the basis of such effect, we design a cuboid sample with an appropriate surface decoration. A simulated far-field radiation pattern demonstrates its broadband directional emission (relative bandwidth of 37.72%). Our work provides an idea to control long-wavelength EM wave propagation using a compact structure that possesses a small device size compared to twice wavelength. The reason is that the EM response of such metamaterials is a non-resonant effect relying on the meshes' connectivity. On the other hand, most conventional antennas (for instance, dipole antennas) rely on the interference between scattered waves, and their geometry sizes are usually on the order of a working wavelength. These findings provide a novel way for manipulating a long-wavelength EM wave and designing a miniaturized and integrated directional antenna.

We consider a double mesh metamaterial (DMM) which is composed of two interlaced wire meshes with period a and $w_1 \times w_1$ ($w_1 = 0.05a$) square cross sections. Both metallic meshes (red and blue in Fig. 1(a)) are assumed to be perfect electric conductors (PEC) and separated by $\sqrt{3}/2$ along the (111) direction. Since the DMM has body-centered-cubic (BCC) symmetry, its Wigner–Seitz primitive unit cell is a truncated octahedron (gray in Fig. 1(a)). The corresponding Brillouin zone is a 12-sided rhombic dodecahedron (Fig. 1(b)). Because the two meshes are not connected, they have independent potentials [26]. Their potential difference leads to a low-frequency mode at Brillouin zone corners (H points) rather than at the zone center [28].

The dispersion relation of the DMM is calculated using the commercial software package COMSOL MULTIPHYSIS.

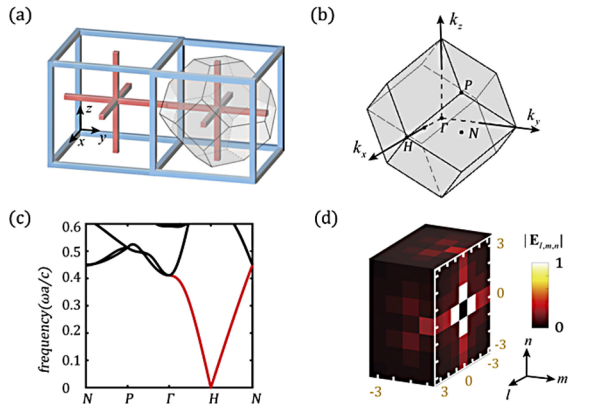

Fig. 1. Double mesh metamaterial (DMM) with index ellipsoid at Brillouin zone corners (H points). Two interlaced meshes (red and blue) form a body-centered-cubic lattice. (a) Wigner–Seitz primitive unit cell (gray) of the DMM. (b) Rhombic dodecahedron Brillouin zone. (c) Dispersion relation. The eigen mode at low frequency emerges from H ($\mathbf{k} \neq 0$). (d) Bloch harmonic amplitudes $|\mathbf{E}_{l,m,n}|$ of the eigen mode at $(k_x, k_y, k_z) = (0, 0, 0.02) \cdot (2\pi/a)$. The normalized Bloch harmonics have maximal amplitude $|\mathbf{E}_{\pm1,0,0}|$, $|\mathbf{E}_{0,\pm1,0}|$, $|\mathbf{E}_{0,0,\pm1}|$, while $|\mathbf{E}_{0,0,0}|$ is very small.

Different from ordinary materials, for instance air, its lowest frequency band emerges from the H point with a linear dispersion as shown in Fig. 1(c), indicating an index ellipsoid is centered at the Brillouin zone corner (H points). To confirm this property, we calculate the Fourier spectrum of an eigen mode at $(k_x, k_y, k_z) = (0.02, 0, 0) \cdot 2\pi/a$. As shown in Fig. 1(d), the Bloch harmonics $\mathbf{E}_{l,m,n}$ of the eigen mode has maximal amplitudes on six cubes with $|\mathbf{E}_{\pm1,0,0}|$, $|\mathbf{E}_{0,\pm1,0}|$, and $|\mathbf{E}_{0,0,\pm1}|$, while $|\mathbf{E}_{0,0,0}|$ is negligibly small. It indicates that this eigen mode of the DMM is near the H point rather than the Γ point.

This index ellipsoid at the nonzero $\mathbf{k}$-point can lead to an anomalous wave refraction when the DMM is truncated along different surface orientations, the so-called orientation-dependent coupling effect [26]. We note that such orientation-dependent effect is a broadband effect since index ellipsoids near Brillouin zone corners (H points) occur near the zero-frequency. When the DMM is truncated and bounded by an ordinary material with index ellipsoid at zero $\mathbf{k}$-point, the EM wave refraction behavior is determined by the conservation of the $\mathbf{k}_{\parallel}$-component. Different refraction phenomena would occur depending on the different surface orientations, which can be illustrated using the equifrequency diagram in Fig. 2. For the case of the (001) orientation, the index ellipsoids at the H point (red spheres, Fig. 2(a)) are projected onto $\bar{\Gamma}$ (the surface Brillouin zone center). The equifrequency surfaces of the DMM and the one of air share a common $\mathbf{k}_{\parallel}$-component. It means that a normal incident plane wave from air can excite the propagating mode in the DMM and vice versa. In order to verify this, we calculate the electric field pattern of a DMM slab with a finite thickness of $10a$ (Fig. 2(d)). A plane wave is normally impinged onto the DMM. However, when the DMM is truncated along the (110) orientation (Fig. 2(b)), the index ellipsoids at H are projected onto the $\bar{N}$ point (on the surface Brillouin zone edge). Momentum conversation forbids the EM coupling between the DMM and air. That is to say, a normal incident wave from the air cannot excite the propagating mode in the DMM (Fig. 2(e)). After a similar analysis, one finds that, for the case of the (111) orientation, the

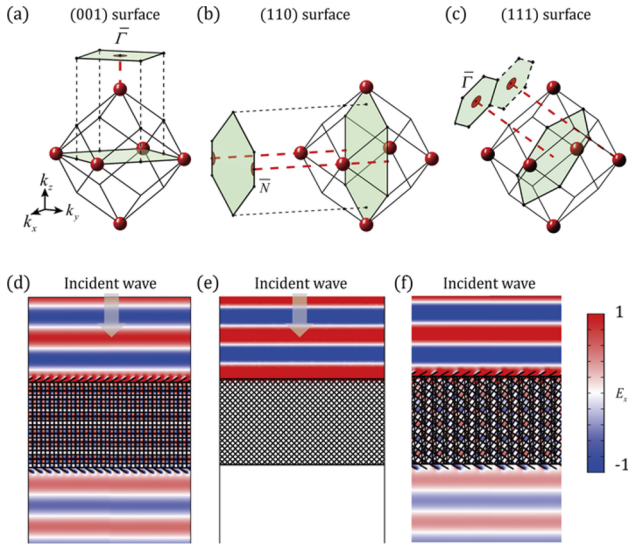

Fig. 2. Orientation-dependent coupling effect between DMM and air. The index ellipsoids of the DMM are centered at the Brillouin zone corner (red spheres, H points). The surface Brillouin zone is projected onto different surfaces. (a) Surface Brillouin zone when the DMM is truncated along the (001) orientation. The index ellipsoid at H ($\mathbf{k} \neq 0$) is projected onto $\bar{\Gamma}$ (surface Brillouin zone center). (b) Surface Brillouin zone when the DMM is truncated along the (110) orientation. The index ellipsoid is projected onto $\bar{N}$ (hexagon sides). (c) Surface Brillouin zone when DMM is truncated along (111) orientation. The index ellipsoid is projected onto $\bar{\Gamma}$ (surface Brillouin zone center). (d) Simulated electric field pattern when a plane wave is impinged to the DMM slab from air. The DMM slab is truncated along the (001) orientation. A plane wave with frequency of $0.14c/a$ is normally impinged onto the surface. (e) Simulated electric field pattern when the DMM slab is truncated along the (110) orientation. (f) Simulated electric field pattern when the DMM slab is truncated along the (111) orientation.

plane wave in air also can couple with the propagation mode in the DMM (Fig. 2(f)). Similar analysis can be made for other crystalline surfaces to determine whether EM waves can couple through the surface between the DMM and air.

To observe this orientation-dependent coupling effect, we calculate the transmission spectrum of a 10-layer slab of DMM truncated in the (001) surface as shown in Fig. 3(a). Unexpectedly, the transmission vanishes (red line, Fig. 3(c)) although the $\mathbf{k}_{\parallel}$-components of two materials match. The reason is that the propagating mode in the DMM has an opposite parity to the incident plane wave in air. Figures 3(d) and 3(e) plot the eigen EM fields of a bulk mode at $(k_x, k_y, k_z) = (0, 0, 0.02) \cdot 2\pi/a$. The electric field has a concentric form, since two interlaced meshes have different potentials. Meanwhile, the magnetic field forms a vortex around the metallic wire due to the electric current on the meshes. These opposite parities forbid the coupling between air and DMM leading to total reflection. To enable the EM wave coupling between air and DMM, one can introduce some symmetry-breaking decoration [27] on the surface of the DMM, such as by attaching a tilted metallic rod (Fig. 3(b)). To confirm this, we calculated the transmission for a 10-layer slab of DMM with the surface decoration (black line, Fig. 3(c)). The transmission spectrum exhibits a series of transmission peaks as the consequence of the Fabry–Perot interference due to the partial reflection on both surfaces.

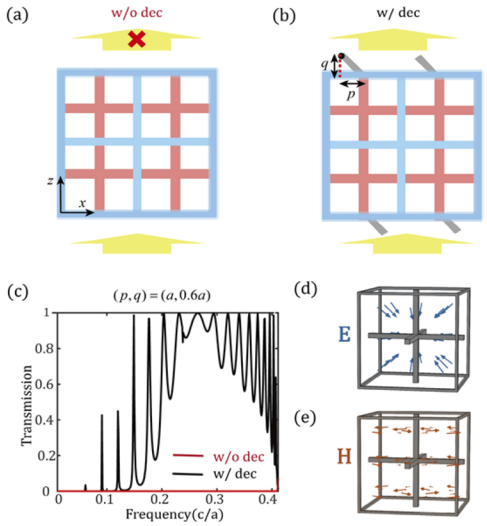

Fig. 3. Dark mode excitation via surface decoration on the (001) surface. (a) Sketch of DMM sample truncated along the (001) direction without a surface decoration. (b) DMM with a symmetry-breaking surface decoration. The crystal surface is decorated by attaching a tilted metallic rod. The end of the rod is at (p, q). (c) Transmission for undecorated (red) and decorated (black) DMMs with 10 periods. (d) and (e) Electromagnetic field of the eigen mode at $f = 0.033c/a$.

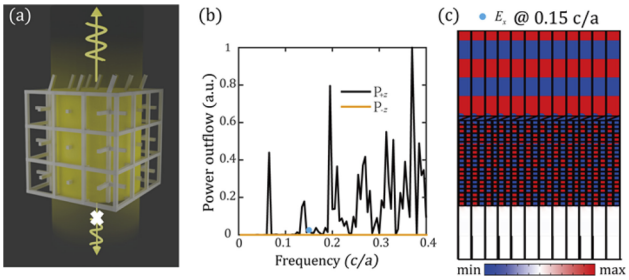

Fig. 4. Broadband directional emission of a DMM slab. (a) Sketch of the DMM slab embedded in air. The EM wave in the DMM can couple out through the decorated surface (upper surface), whereas it cannot couple out through the undecorated surface (lower surface). (b) Power outflow spectra for the $+z$ direction (black) and $-z$ direction (orange). (c) Simulated electric field pattern at the frequency of $0.15c/a$.

This feature implies that by introducing a surface decoration or not, we can control the EM wave emission from the DMM inside. For instance, we consider a DMM slab with finite thickness in the z direction which is periodic in x and y directions. Its upper surface is decorated, while its lower surface is not. Then we put a point source (effectively a square array) into the DMM. The excited bulk mode in the DMM can only couple out through the upper surface, resulting in a directional emission in the $+z$ direction (Fig. 4(a)).

As calculated in Fig. 4(b), the power outflow in the $+z$ direction is much bigger than that in the $-z$ direction in a wide frequency range. Due to the impedance mismatch between DMM and air, the spectra of the $+z$ direction exhibit several Fabry–Perot resonance peaks (black line in Fig. 4(b)). However, the directional emission effect is a broadband effect even when the emission efficiency is relatively low at some frequencies.

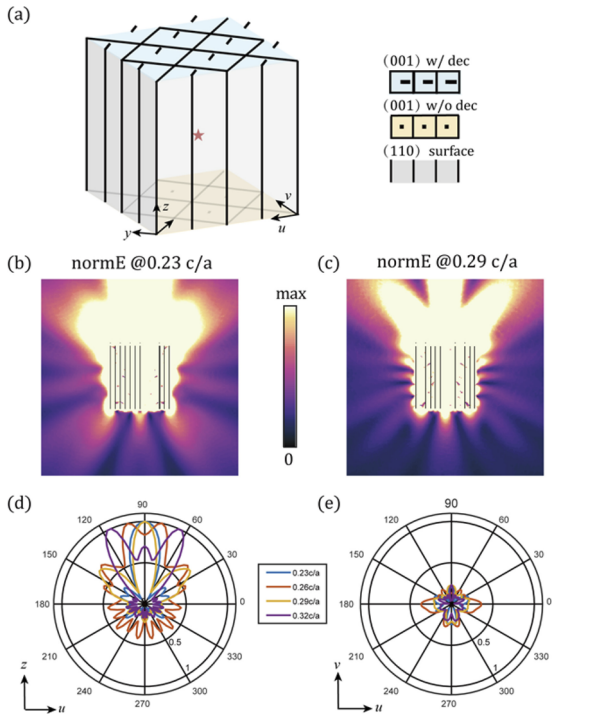

Fig. 5. Directional emission of a cuboid DMM. (a) Cuboid sample of the DMM. The upper and lower surfaces of the cuboid are (001) surfaces while the four-side surfaces are (110) surfaces. The upper surface is decorated by tilted rods. A line source (red star) is placed at the center of the cuboid. (b) and (c) Simulated electric field patterns at $f = 0.23c/a$ and $f = 0.29c/a$, respectively. The EM wave can only be coupled out through the upper surface with a decoration. (d) and (e) Far-field radiation patterns on the uoz plane and the uov plane.

Figure 4(c) exemplifies the case at the frequency of $0.15c/a$, where most of the emitted waves propagate in the $+z$ direction.

Taking advantage of the orientation-dependent coupling effect and the symmetry-breaking surface decoration, we can, in principle, use the DMM structure to manipulate the low-frequency wave's propagation behavior in a fruitful way. On the other hand, since the DMM works at a long-wavelength limit, its small overall size (compared to twice wavelength) is favorable in miniaturized microwave devices. For example, we can design a cuboid DMM to realize the broadband directional emission (Fig. 5(a)). The upper surface and the lower surface of the cuboid DMM are truncated in the (001) direction, while other four-side surfaces are truncated in the (110) direction. Tilted metallic rods are added only on the upper surface. According to the analysis above, the EM wave inside the structure can only radiate in the $+z$ direction. An E_z-polarized line source (a red star) is put inside the DMM cuboid. Figures 5(b) and 5(c) simulate the excited electric field pattern at frequencies of $0.23c/a$ and $0.29c/a$.

Since the orientation-dependent coupling is a broadband effect in low frequency, this type of directional radiation should work in a relatively broad frequency regime. The far-field radiation in uoz and uov planes is calculated in Figs. 5(d) and 5(e). As expected, the radiations from the DMM cuboid are concentrated in the $+z$ direction within a wide frequency range from $0.23c/a$ to $0.32c/a$ relative bandwidth of 37.72%. One can narrow the radiation beam width to make it more directional, such as by decreasing DMM's filling ratio or by using a background material with a higher index.

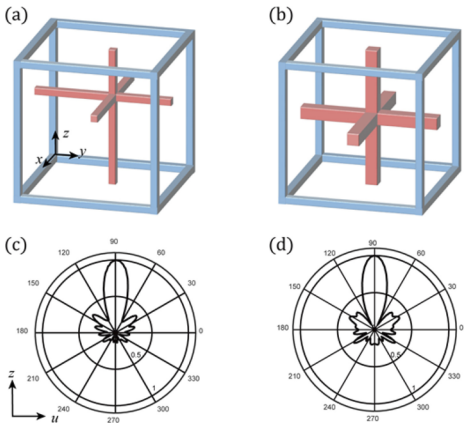

Fig. 6. Robust emission against the global defect. Two cases are considered here. (a) Offset of one mesh. One mesh's center (red) is shifted to (0.01a, 0.02a, 0.03a). (b) Modification of the bar width. One mesh's bar is modified as $w_2 = 0.07a$. (c) and (d) Simulated far-field radiation pattern at the frequency of $0.23c/a$.

In addition, this directional emission phenomenon is robust against small perturbations for the reason that the EM response is governed by global connectivity of meshes. In order to verify this, we introduce global defects to the DMM cuboid. In Fig. 6(a), one of the meshes is shifted to $(0.01a, 0.02a, 0.03a)$ breaking the BCC symmetry of the structure. On the other hand, Fig. 6(b) modifies one mesh's bar width to $w_2 = 0.07a$. For both cases, most of the waves are emitted to the $+z$ direction, indicating that the directional emission effect of the DMM is robust to defect to some extent.

In summary, we investigate the orientation-dependent coupling effect of 3D connection-type metamaterials. We find that low-frequency bulk modes are anti-symmetric and cannot couple with the plane wave. To enable their coupling, we introduce a symmetry-breaking surface decoration. A cuboid DMM with an appropriate surface decoration is designed to demonstrate its broadband directional emission. The robustness of the directional emission is demonstrated by introducing global defects to the DMM cuboid. Our work provides a scheme to manipulate a long-wavelength EM wave with compact structure. Our scheme may inspire the design of miniaturized directional antennas in the microwave region.

Funding. National Key Research and Development Program of China (2019YFA0706302, 2022YFA1404304); Guangdong Basic and Applied Basic Research Foundation (2023B1515040023).

Acknowledgment. This work has been supported by the National Science Foundation and Guangdong Basic and Applied Basic Research Foundation.

Disclosures. The authors declare no conflicts of interest.

Data availability. Data underlying the results presented in this paper are not publicly available at this time but may be obtained from the authors upon reasonable request.

REFERENCES

1. J. B. Pendry, A. J. Holden, W. J. Stewart, *et al.*, Phys. Rev. Lett. **76**, 4773 (1996).
2. J. B. Pendry, A. J. Holden, D. J. Robbins, *et al.*, IEEE Trans. Microwave Theory Tech. **47**, 2075 (1999).
3. D. R. Smith, J. B. Pendry, and M. C. K. Wiltshire, Science **305**, 788 (2004).
4. C. M. Soukoulis and M. Wegener, Nat. Photonics **5**, 523 (2011).
5. D. R. Smith, W. J. Padilla, D. C. Vier, *et al.*, Phys. Rev. Lett. **84**, 4184 (2000).
6. S. Linden, C. Enkrich, M. Wegener, *et al.*, Science **306**, 1351 (2004).
7. R. A. Shelby, D. R. Smith, and S. Schultz, Science **292**, 77 (2001).
8. C. Luo, S. G. Johnson, J. D. Joannopoulos, *et al.*, Phys. Rev. B **65**, 201104 (2002).
9. J. B. Pendry, Phys. Rev. Lett. **85**, 3966 (2000).
10. N. Garcia and M. Nieto-Vesperinas, Phys. Rev. Lett. **88**, 207403 (2002).
11. D. Maystre and S. Enoch, J. Opt. Soc. Am. A **21**, 122 (2004).
12. J. B. Pendry, D. Schurig, and D. R. Smith, Science **312**, 1780 (2006).
13. U. Leonhardt, Science **312**, 1777 (2006).
14. D. Schurig, J. J. Mock, B. J. Justice, *et al.*, Science **314**, 977 (2006).
15. S. Enoch, G. Tayeb, P. Sabouroux, *et al.*, Phys. Rev. Lett. **89**, 213902 (2002).
16. P. Moitra, Y. Yang, Z. Anderson, *et al.*, Nat. Photonics **7**, 791 (2013).
17. Y. Yuan, L. F. Shen, L. X. Ran, *et al.*, Phys. Rev. A **77**, 053821 (2008).
18. S. I. Maslovski, S. A. Tretyakov, and P. A. Belov, Microw. Opt. Technol. Lett. **35**, 47 (2002).
19. P. A. Belov, R. Marques, S. I. Maslovski, *et al.*, Phys. Rev. B **67**, 113103 (2003).
20. I. S. Nefedov, A. J. Viitanen, and S. A. Tretyakov, Phys. Rev. E: Stat., Nonlinear, Soft Matter Phys. **71**, 046612 (2005).
21. M. G. Silveirinha and C. A. Fernandes, IEEE Trans. Microwave Theory Tech. **53**, 1418 (2005).
22. J. Shin, J. T. Shen, and S. Fan, Phys. Rev. B **76**, 113101 (2007).
23. S. I. Maslovski and M. G. Silveirinha, Phys. Rev. B **80**, 245101 (2009).
24. C. R. Simovski, P. A. Belov, A. V. Atrashchenko, *et al.*, Adv. Mater. **24**, 4229 (2012).
25. H. Latioui and M. G. Silveirinha, Phys. Rev. B **96**, 195132 (2017).
26. W. J. Chen, B. Hou, Z. Q. Zhang, *et al.*, Nat. Commun. **9**, 2086 (2018).
27. A. W. Powell, R. C. Mitchell-Thomas, S. Zhang, *et al.*, ACS Photonics **8**, 841 (2021).
28. D. Sakhno, E. Koreshin, and P. A. Belov, Phys. Rev. B **104**, L100304 (2021).
29. Z. L. Liao, W. M. Deng, Z. L. Xiang, *et al.*, Front. Phys. **10**, 1 (2022).
30. Q. H. Yan, R. J. Liu, Z. B. Yan, *et al.*, Nat. Phys. **14**, 461 (2018).
31. Y. Wang, X. Zhou, S. Li, *et al.*, Sci. Rep. **11**, 8684 (2021).
32. H. Wang, Q. Chen, O. Zetterstrom, *et al.*, Appl. Sci. **11**, 7153 (2021).